Macromolecules

pubs.acs.org/Macromolecules Article

Revealing the Molecular-Level Interactions between Cationic Fluorinated Polymer Sorbents and the Major PFAS Pollutant PFOA

Xiao Tan, Michał Sawczyk, Yixin Chang, Yiqing Wang, Adil Usman, Changkui Fu, Petr Král, Hui Peng, Cheng Zhang,* and Andrew K. Whittaker*

Cite This: *Macromolecules* 2022, 55, 1077−1087 Read Online

ACCESS | Metrics & More | Article Recommendations | Supporting Information

ABSTRACT: The development of new technologies for the removal of a family of manufactured chemicals, the per- and polyfluoroalkyl substances (PFAS), from the environment is urgently needed to safeguard public and environmental health. Here we report a fundamental study of the binding mechanisms driven by fluorine−fluorine and electrostatic interactions between perfluorooctanoic acid (PFOA), an important PFAS molecule, and three types of block copolymer sorbents containing individually perfluoropolyether (PFPE) or quaternized ammonium groups, or both functional segments in combination. The results show that both the fluorine−fluorine interactions between the PFPE segment of the block copolymer and the fluorinated tail of the PFOA as well as electrostatic attraction between the quaternized ammonium group and the anionic PFOA headgroup are crucial to achieve effective PFOA sorption from aqueous solutions. The fluorine−fluorine interactions contribute to recognition of PFOA molecules via fluorophilicity, with fast exchange between bound and free PFOA being observed, while the electrostatic interactions can tightly bind PFOA, thus precluding such exchange. Both types of interaction are observed to be rapidly established within 5 min. We show that the sorbents containing both fluorinated and cationic groups have a higher PFOA removal efficiency with potentially improved sorption capacity compared with the sorbents with a single functional group and that the electrostatic attraction is stronger and dominates the fluorine−fluorine interactions when the sorbent is highly charged. Overall, these results provide important insights into designing novel sorbents for rapid and efficient PFAS removal from contaminated environments.

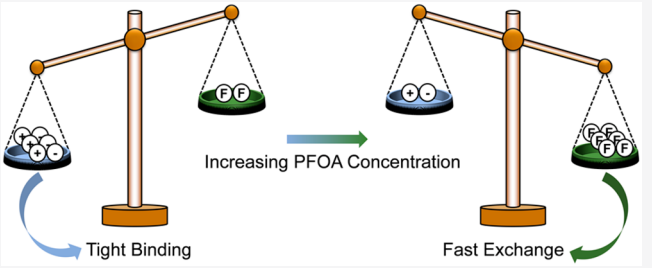

INTRODUCTION

Per- and polyfluoroalkyl substances (PFAS) are a group of man-made chemicals that can travel long distances through soil and water and do not readily break down in the environment.[1−5] Their highly persistent nature and demonstrated high affinity for biological membranes have raised wide concern for their potential to damage human health.[6−9] The development of strategies for the removal of PFAS from contaminated water sources is therefore of great interest.[10,11] Conventional methods of removal of organic pollutants such as the use of activated carbon, anion exchange resins, and membrane filtration have been actively investigated over the past decade. However, despite some degree of success, these technologies have certain limitations, including low PFAS removal efficiency due to interference from other contaminants, e.g., salts and organic matters,[12−14] and a general lack of removal selectivity.[14−16]

Fluorinated polymer sorbents can potentially address the limitations of current approaches for removal of PFAS under real-life conditions.[17−21] The key to the success of such fluorinated sorbents is the combination of mechanisms that leverage fluorophilic interactions and electrostatic attraction. The combination of the two interactions promises to improve removal efficiency and capacity for all classes of PFAS including short-chain and neutral PFAS. Previous work has highlighted the importance of fluorinated segments in sorbents. For example, Koda et al. proposed fluorinated microgel star polymers for selective capture of PFAS in ethanol/deuterium oxide (D_2O) (1:1, v/v). Interactions between the star polymers and perfluorooctanoic acid (PFOA) were characterized by ^{19}F NMR, showing changes in chemical shift of the main peak from PFOA from −82.4 to −82.6 ppm with broader line widths observed after sorption.[17] Shetty et al. designed fluorine-rich calixarene-based porous polymers for removal of PFOA from water.[18] Compared with the non-fluorinated polymers having 23−64% PFOA removal efficiency, the fluorinated polymers exhibited improved removal efficiency of 79−100%. This increase is attributed to hydrophobic fluorine−fluorine interactions between the

Received: November 25, 2021
Revised: January 5, 2022
Published: January 14, 2022

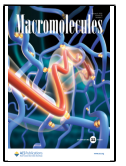

https://doi.org/10.1021/acs.macromol.1c02435
Macromolecules 2022, 55, 1077−1087

adsorbents and PFOA. More recently, Leibfarth et al.[20] reported the preparation of ionic fluorogels using a commercially available perfluoropolyether (PFPE) with dimethacrylate chain-end functionality and a quaternary ammonium monomer. The gel demonstrates >80% removal efficiency for both long- and short-chain PFAS in deionized water in the presence of humic acid, which is superior to conventional strategies. These reports highlight that both the fluorine−fluorine and electrostatic attractions are important for selective and efficient PFAS removal from the aqueous solutions. However, a detailed fundamental understanding of the mechanisms of interaction between cationic fluorinated sorbent and PFAS is still absent.

In our previous work,[22] we reported effective sorption of PFOA at high concentrations by uncharged amphiphilic PFPE-containing block copolymers in phosphate buffered saline. The materials demonstrated an effective PFOA removal of up to 90%, with fast exchange between free and bound PFOA being observed after sorption. In this study, we aim to investigate the role of both fluorine−fluorine and electrostatic interactions in the sorption from aqueous solution of one of the most extensively used PFAS, PFOA. The interactions and behavior of the species in solution were studied by using molecular dynamics simulations, ^{19}F NMR, dynamic light scattering, and isothermal titration calorimetry. Block copolymers with PFPE as the fluorinated segment were prepared by reversible addition−fragmentation chain-transfer (RAFT) polymerization. An amine-containing monomer 2-(dimethylamino)ethyl acrylate (DMAEA) was included in the second block to provide cationic units after quaternization with iodomethane. Three different polymer sorbents were prepared, namely nonionic PFPE, cationic PFPE, and cationic non-PFPE sorbents, and tested for sorption of PFOA from pure water. Our results reveal different interaction mechanisms involving fluorine−fluorine and electrostatic interactions—dynamic binding with fast exchange vs tight binding without exchange. The study also confirms that at low PFOA concentrations electrostatic attractions are superior to fluorine−fluorine interactions for sorption of PFOA. It is expected that the current findings will provide important insights into the design and preparation of the next-generation effective PFAS sorbents.

EXPERIMENTAL SECTION

Materials. The hydroxy-terminated perfluorinated poly(propylene ether) (PFPE AL-2, $M_w \sim 2000$ g/mol, CAS Number: 126066-30-6) was obtained from The Chemours Company. Oligo(ethylene glycol)methyl ether acrylate (OEGA, M_w = 480 g/mol) and 2-(dimethylamino)ethyl acrylate (DMAEA) purchased from Sigma-Aldrich were both passed through basic alumina columns to remove inhibitors before use. The RAFT agent 2-(butylthiocarbonothioylthio)propionic acid (BTPA) was synthesized following the procedure reported previously.[23] The initiator 2,2′-azobis(2-methylpropionitrile) (AIBN) was recrystallized twice from methanol before use. Milli-Q water with a resistivity of 18.4 MΩ·cm was used for the sorption experiments. All other chemicals were purchased from Sigma-Aldrich and used as received.

Synthesis of Poly(DMAEA$_6$-*co*-OEGA$_3$)-PFPE (PAO-F). PAO-F block copolymer was synthesized via RAFT polymerization. The PFPE macro-RAFT agent was prepared by using methods described in our previous work.[22,24,25] For a typical polymerization, the PFPE macro-RAFT agent (0.5 g, 0.225 mmol), DMAEA (0.215 g, 1.5 mmol), OEGA (0.36 g, 0.75 mmol), and AIBN (7.39 mg, 0.045 mmol) were dissolved in 2.5 mL of α,α,α-trifluorotoluene (TFT)/dimethylformamide (DMF) (4:1, v/v) solution in a glass round-bottom flask fitted with a magnetic stirrer bar. Argon was used to deoxygenate the solution for 15 min. The reaction mixture was heated to 65 °C and left to react for 3.5 h. The reaction was stopped by placing the round-bottom flask in an ice bath and exposing to air. The reaction mixture was concentrated and precipitated into a large excess of cold hexane/diethyl ether (1:1), followed by centrifugation. The purification cycle was repeated three times, and the product, PAO-F, was obtained by evaporating the excess solvent under high vacuum at room temperature for 24 h. The synthetic procedures for poly-(OEGA)$_7$-PFPE (PO-F) and poly(DMAEA)$_{16}$-ethyl (PA) can be found in the Supporting Information.

Preparation of PAO-F+. In a typical quaternization reaction, iodomethane (0.189 g, 0.083 mL) was added to a solution of PAO-F (0.5 g) dissolved in DMF (5 mL) with stirring at room temperature. The solution mixture was then heated to 50 °C and reacted for 24 h in the dark. The polymer was purified by precipitation into a large excess of diethyl ether, followed by evaporation of the solvent under vacuum, and dialyzed against Milli-Q water for 24 h. The quaternized product, PAO-F+, was obtained by freeze-drying. The same quaternization procedure was used to produce PA+.

Interactions between PFOA and Polymer Sorbents. Sorption of PFOA by the three polymers was characterized by using 1D ^{19}F NMR and 2D ^{19}F diffusion-ordered spectroscopy (DOSY) techniques. For PO-F and PAO-F+, 5 mg of the polymer was dissolved in 5 mL of Milli-Q water to give a polymer stock solution of concentration of 1 mg/mL, with each solution having the same total fluorine content. For PA+, to achieve the same concentration of ammonium groups as the PAO-F+, 3.3 mg of the polymer was dissolved in 10 mL of Milli-Q water, resulting in a polymer stock solution of concentration 0.33 mg/mL. PFOA stock solutions (3 mg/mL) were prepared by dissolving 9 mg of PFOA in 3 mL of Milli-Q water. The solutions for measurement were prepared as follows: an aliquot of 510 μL of the polymer stock solution was mixed separately with 22.5, 52.5, 67.5, 90, and 142.5 μL of the PFOA stock solution. 400 μL of each solution mixture was collected and measured by ^{19}F NMR spectroscopy using a coaxial insert filled with D_2O for the NMR lock signal. The solution mixtures of PFOA and the two PFPE-containing polymers (i.e., PO-F and PAO-F+) were further analyzed for ^{19}F NMR DOSY by using the same coaxial insert. 510 μL of Milli-Q water mixed with 22.5 μL of the PFOA stock solution was also prepared and measured by using ^{19}F NMR and ^{19}F NMR DOSY as control experiments.

Changes in Polymer Size and ζ Potential on Addition of PFOA. Dynamic light scattering (DLS) was used to monitor the changes in polymer size and ζ potential during stepwise addition of the above PFOA stock solution (3 mg/mL) to solutions of each type of polymer sorbent. For a typical DLS experiment, a total number of 19 additions of PFOA, with each addition volume being 15 μL, were added to 1020 μL of polymer solution in a polystyrene cuvette. After each addition, the solution was thoroughly mixed by using a pipet, followed by size measurement. Initial sizes of the three polymers were also measured. The ζ potential experiments were conducted in a folded capillary zeta cell following the same protocols as above. The ζ potential of the three polymer sorbents after quaternization prior to the addition of PFOA was also measured.

Interaction Duration and Thermodynamic Properties. The calorimetric data were obtained by using a nano-isothermal titration calorimetry (ITC) calorimeter from TA Instruments. All of the solutions were thoroughly degassed before measurement. The sample cell was filled with 300 μL of polymer solution at 1 mg/mL for PO-F and PAO-F+ and 0.33 mg/mL for PA+. The titration was performed by injecting 2.51 μL of PFOA solution (3 mg/mL) into the sample cell under continuous stirring at 25 °C. The effective volume of the sample cell was 170 μL. Control experiments were conducted for each ITC experiment by titrating PFOA solution into the sample cell filled with 300 μL of Milli-Q water. The program NanoAnalyze was used to analyze the data, and thermograms were obtained by subtracting the data from the control experiments.

Characterization Methods. *Nuclear Magnetic Resonance (NMR).* All NMR experiments were conducted on a Bruker AVANCE

https://doi.org/10.1021/acs.macromol.1c02435
Macromolecules 2022, 55, 1077−1087

Scheme 1. Synthetic Scheme for PO-F, PAO-F+, and PA+

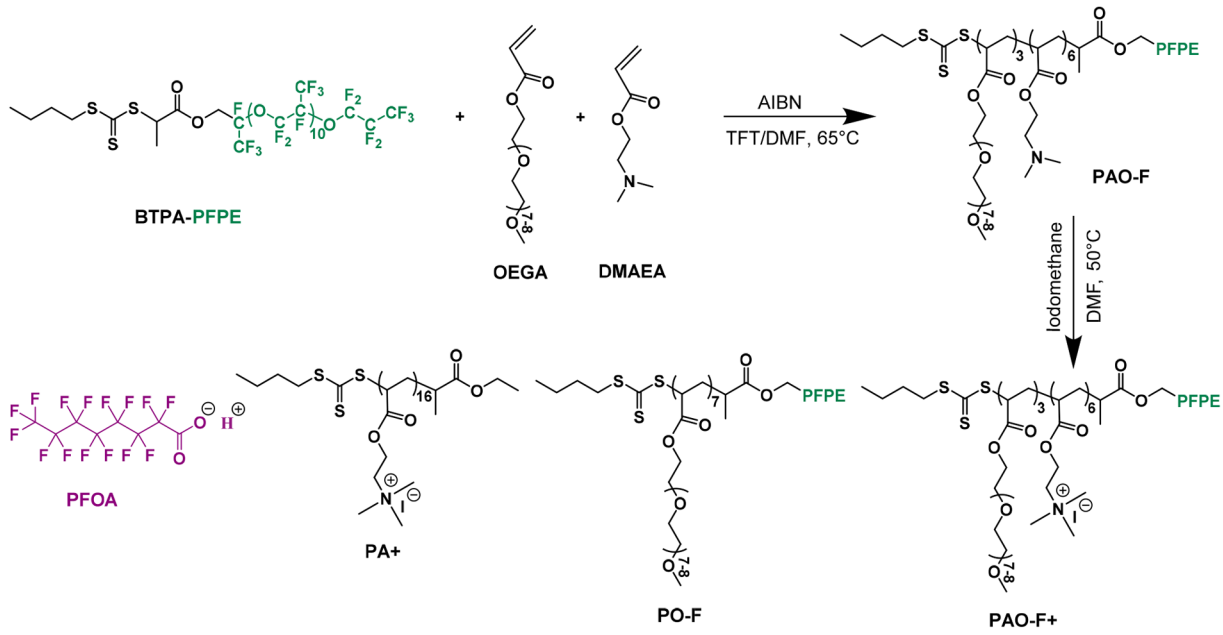

400 MHz (9.4 T) spectrometer at 25 °C. ^{1}H NMR spectra of the polymer solutions were acquired in either $CDCl_3$ or DMSO-d_6: a 90° pulse width of 14 μs, relaxation delay of 1 s, acquisition time of 4.1 s, and 32 scans were used in all measurements. ^{19}F NMR spectra were acquired by using $CDCl_3$, DMSO-d_6, or Milli-Q as the solvent. Coaxial inserts filled with D_2O were used for the measurement of samples dissolved in Milli-Q water. Spectra were measured under the following conditions: 90° pulse width 15 μs, relaxation delay 2 s, acquisition time 0.73 s, and 128 (in $CDCl_3$ or DMSO-d_6) or 3000 (in Milli-Q water) scans. ^{19}F NMR DOSY was conducted under the following conditions: relaxation delay 2 s, diffusion time (Δ) 0.3 s, gradient time (δ) 0.003 s, and the number of scans 800.

Size Exclusion Chromatography (SEC). Molecular weights and molecular weight distributions were measured by SEC using a Polymer Laboratories GPC50 Plus equipped with a differential refractive index detector. HPLC grade *N*,*N*-dimethylacetamide (DMAc) containing 0.03 wt % LiCl was used as the mobile phase at a flow rate of 1 mL/min. InfinityLab EasiVial polystyrene standards were used for the column calibration. Two PLGel Mixed B (7.8 × 300 mm^2) columns connected in series were held at a constant temperature of 50 °C for separations. Samples were freshly prepared in DMAc + 0.03 wt % LiCl at a concentration of 5 mg/mL and then passed through 0.45 μm PTFE filters prior to measurement.

MD Simulations. Fully atomistic models of PO-F, PAO-F+, PA+, and PFOA were generated by using GaussView. The MD simulations of the polymers (10 molecules of each polymer) with or without presence of PFOA were conducted in a 15 × 15 × 15 nm^3 simulation box filled with water. Potassium counterions were added to neutralize the system. The number of PFOA molecules in the simulation box was 18 for the self-assembled PO-F and PAO-F+ (mole ratio of PFOA:polymer = 1.8) and 46 for the single-chain folding PA+ (mole ratio of PFOA:polymer = 4.6). For each of the systems, trajectories over 100 ns were collected. All the MD simulations were performed by using the NAMD code and described with the CHARMM general force field.[26−28] Long-range Coulombic interactions were evaluated by using the particle mesh Ewald (PME) method.[29] The simulations were performed in the NpT ensemble at p = 1 bar and temperature T = 298 K by using Langevin dynamics with a damping constant of 1 ps^{-1} and a time step of 2 fs.

Dynamic Light Scattering (DLS). DLS was conducted by using a Nanoseries Zetasizer (Malvern, UK) containing a 2 mW He−Ne laser operating at a wavelength of 633 nm. The scattering angle used was 173°. The number of runs per measurement was set as automatic, and the number of measurements for each test was five. BRAND semi-microcuvettes made of polystyrene with a minimum filling volume 1.5 mL were used for the measurements.

The ζ potential was measured on the Nanoseries Zetasizer (Malvern, UK) instrument using a DTS1070 folded capillary zeta cell. The number of runs per measurement ranged from 20 to 50. For each test, five repeated measurements were conducted.

Nano-Isothermal Titration Calorimetry (ITC). ITC experiments were performed on a Nano ITC Low Volume isothermal titration calorimeter from TA Instruments. The temperature was set to 25 °C, the volume of each injection was 2.51 μL, the total number of injections was 19, the injection interval was 250 s, the stirring rate was set as 300 rpm, and a duration of 60 s was used for the initial baseline and 120 s for the final baseline.

RESULTS AND DISCUSSION

In this work, we aim to systematically investigate the important roles of fluorine−fluorine and electrostatic interactions for effective sorption of one of the most commonly used PFAS, PFOA, by a novel block copolymer system. As the pK_a of PFOA is lower than 1,[30,31] PFOA mainly exists in its anionic form in Milli-Q water (pH ≈ 7) (Scheme 1). Before discussing the unique interactions between various polymer sorbents and PFOA, we briefly describe the synthesis of a series of fluorinated and quaternized polymers (Scheme 1). First, two macro-chain-transfer agents, perfluoropolyether (PFPE)- and ethyl-modified 2-(butylthiocarbonothioylthio)propionic acid (BTPA), were synthesized by the coupling esterification reaction of *N*-(3- (dimethylamino)propyl)-*N*′-ethylcarbodiimide hydrochloride/4-(dimethylamino)pyridine (EDCl/DMAP). The successful synthesis of the two RAFT agents was confirmed by ^{1}H and ^{19}F NMR as shown in Figures S1−S3.

Three candidate polymer sorbents were synthesized by using RAFT polymerization starting from either the PFPE- or ethyl-modified macro-chain-transfer agent, i.e., two perfluoropolyether (PFPE)-containing block copolymers poly(oligo(ethylene glycol)methyl ether acrylate)$_7$-PFPE (PO-F) and poly((2-dimethylaminoethyl acrylate)$_6$-*co*-OEGA$_3$)-PFPE (PAO-F), as well as a polymer lacking the PFPE block,

https://doi.org/10.1021/acs.macromol.1c02435
Macromolecules 2022, 55, 1077−1087

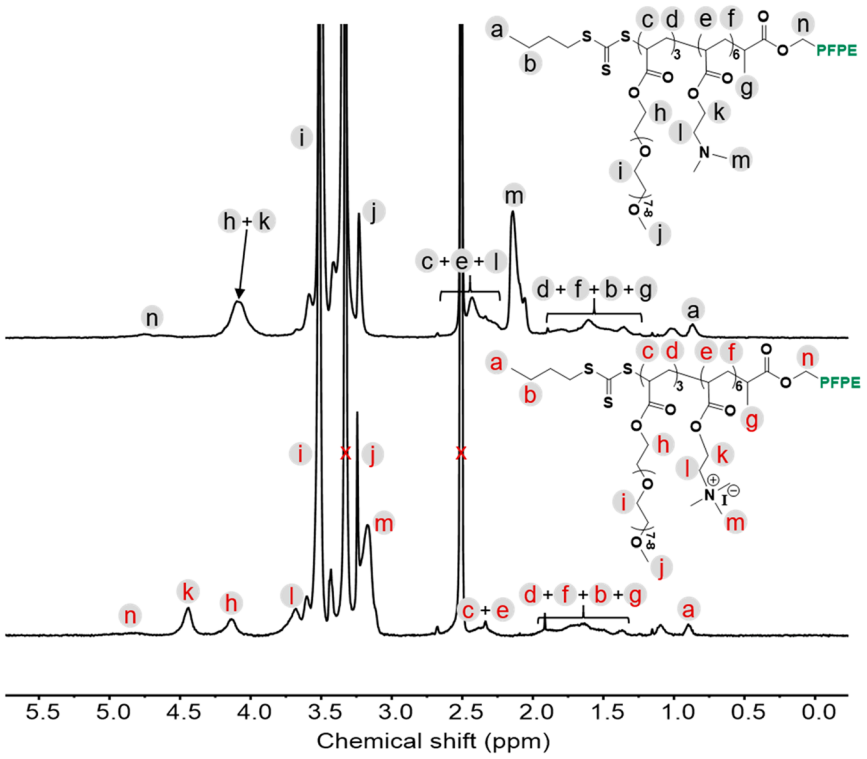

Figure 1. Chemical structures and ^{1}H NMR spectra of PAO-F (top) and PAO-F+ (bottom). Both spectra were measured in DMSO-d_6.

Table 1. Molecular Characterization of the Three Sorbent Polymers

polymer	$DP_{DMAEA/OEGA}$ [a]	$M_{n,NMR}$ [a] (g/mol)	$M_{n,SEC}$ [b] (g/mol)	$Đ$ [b]	ζ [c] (mV)	^{19}F content [d] (wt %)
PO-F	0/7	5600	3800	1.06	0.3	24.4
PAO-F+	6/3	4500	3700	1.17	30.7	25.3
PA+	16/0	2600	1300	1.11	3.3	0

[a]The degree of polymerization (DP) and $M_{n,NMR}$ for each type of polymer were calculated by integrating the terminal methyl group belonging to BTPA (peak a) and the methylene protons next to the ester group (Figure 1, Figures S4 and S6). [b]$M_{n,SEC}$ and $Đ$ were acquired by size exclusion chromatography in *N*,*N*-dimethylacetamide using a RI detector. [c]Determined by DLS after quaternization. [d]The weight percentage of fluorine after quaternization.

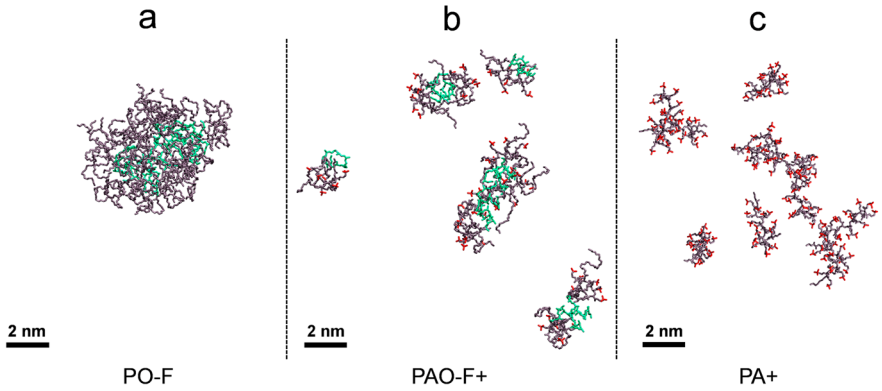

Figure 2. Snapshots of the MD simulations of (a) PO-F, (b) PAO-F+, and (c) PA+ in water taken at 100 ns. Green: PFPE units; gray: OEGA chains; red: quaternary ammonium groups.

poly(DMAEA)$_{16}$-ethyl (PA). After purification to remove unreacted monomer, both ^{1}H NMR and ^{19}F NMR spectra confirmed the successful synthesis of the three polymers (Figure 1 top; Figures S4–S6, top). Taking PAO-F as an example, the methylene protons (2H, $-CH_2O-$) adjacent to the ester groups of DMAEA and OEGA overlap and contribute to a single broad peak at 4.1 ppm (protons h and k in Figure 1, top). Quaternization of PAO-F and PA was then conducted by reaction with iodomethane to produce PAO-F+ and PA+. The NMR peak due to the methylene protons next to ester of the quaternized DMAEA side chains shifted from 4.1 to 4.5 ppm (peak k in Figure 1) after quaternization, while the peak from the methylene protons belonging to OEGA remain unchanged (peak h, Figure 1). The resonance due to the two methyl

https://doi.org/10.1021/acs.macromol.1c02435
Macromolecules 2022, 55, 1077−1087

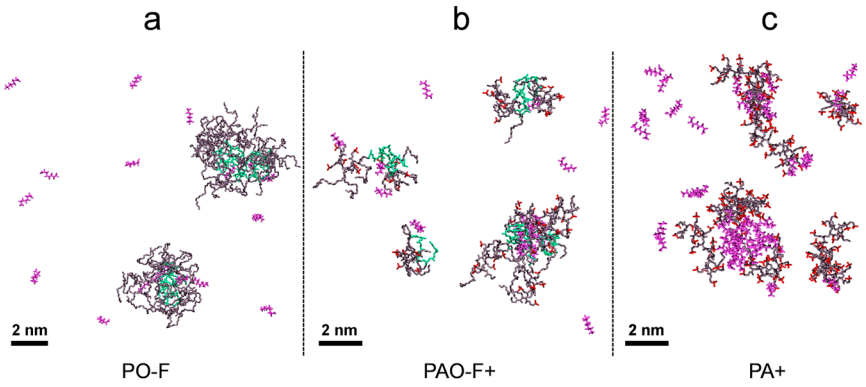

Figure 3. Snapshots from the MD simulations of PFOA and polymer mixture solutions at 100 ns: (a) PO-F, (b) PAO-F+, and (c) PA+. Green: PFPE units; gray: OEGA chains; red: quaternary ammonium groups; purple: PFOA molecules.

terminal groups of DMAEA was also shifted from 2.1 to 3.2 ppm (peak m) after the reaction with iodomethane, demonstrating the successful quaternization and production of PAO-F+ and PA+ (Figures 1, bottom, and Figure S6, bottom).[32,33] All polymers have a low molar mass dispersity determined by using size exclusion chromatography ($Đ$ < 1.2, Table 1). See Table 1 for a comprehensive tabulation of characterization data.

Molecular dynamics (MD) simulations confirm that PO-F and PAO-F+ can self-assemble into micellar structures and that PA+ is stabilized in a single-chain folded conformation in aqueous solution. For each experiment, 10 polymer chains of PO-F, PAO-F+, and PA+ were randomly placed in a 15 × 15 × 15 nm^3 simulation box filled with water molecules. In Figures 2a−c, the PFPE hydrophobic segments are highlighted in green, OEGA in gray, and quaternary ammonium groups in red. The results in Figures 2a,b confirm the formation of multichain aggregates with PFPE segments as the core for PO-F (10 chains) and PAO-F+ (two or three chains). Importantly, the presence of electrostatic repulsion due to the quaternary ammonium groups reduces the size of PAO-F+ aggregates, which contain fewer polymer chains per aggregate compared with PO-F. Multichain aggregates were not observed in the case of PA+, indicating that unimers are the dominant form for such non-fluorinated quaternized polymer in aqueous solution (Figure 2c).

The MD simulations presented here highlight the hydrophobic and electrostatic interactions between PFOA and the polymer sorbent. Figures 3a and 3b clearly show that the PFOA molecules can be sorbed by the PFPE segments of PO-F and PAO-F+ due to the hydrophobic interactions. The large self-assembled PO-F aggregates in free solution become smaller in the presence of PFOA (Figure 3a). This is a result of electrostatic repulsion after the sorption of anionic PFOA, as discussed in the later sections. Sorption of PFOA by the quaternary ammonium groups was also observed in PAO-F+ and PA+ driven by electrostatic attractions (Figures 3b and 3c), leading to increased particle sizes especially for PA+. MD simulations demonstrate that both the PFPE and cationic quaternary ammonium groups can interact with anionic PFOA. The coexistence of hydrophobic and electrostatic interactions is important for improving the sorption capacity and achieving effective removal of PFOA from aqueous solution.

^{19}F NMR is a powerful technique to probe the interactions between PFOA and polymer sorbent through monitoring changes in NMR chemical shift and peak width.[17,22,34−37] The pH of the Milli-Q water was measured to be ≈7 and used in subsequent preparations of polymer and PFOA solutions. Stock solutions of PO-F and PAO-F+ with the same concentration (1 mg/mL, ∼0.18 mM) were prepared; note that each solution had the same fluorine concentration. The concentration of PA+ stock solution was adjusted to be 0.33 mg/mL (∼0.07 mM) to achieve the same concentration of ammonium groups as in the solution of PAO-F+. The concentration of PFOA used for the ^{19}F NMR experiments was 0.3 mM, which is well below the critical micelle concentration (CMC = 25 mM),[38] indicating that fully solvated PFOA molecules were present. The ^{19}F NMR spectrum of PFOA in pure water in Figure 4a showed well-resolved and sharp ^{19}F peaks that could be clearly assigned. ^{19}F peaks belonging to PFOA are shifted to various extents upon the addition of the polymer sorbents (Figures 4b−4d). For example, peak F(1) due to the terminal $-CF_3$ group of PFOA shifts from −80.7 to −83.0 ppm after the addition of PAO-F+. Peaks F(3), F(4), and F(5) which are located at −121.8, −122, and −122.7 ppm in the absence of polymer also shift and have a tendency to merge (Figure 4c). Changes in chemical shifts of peaks due to PFOA can also be observed upon addition of PO-F and PA+, with for example the F(1) resonance shifting from −80.7 ppm to −81.3 and −82.5 ppm, respectively. Compared with the spectrum of free PFOA shown in Figure 4a, it is clear that the F(1) resonance of PFOA has the largest change in chemical shift in the presence of PAO-F+ compared with the other two polymer sorbents (2.3 ppm vs 0.6 and 1.8 ppm for PO-F and PA+, respectively), suggesting the strongest interactions occur between PFOA and the fluorinated cationic polymer.[17] In addition, changes in the NMR line widths of peaks for PFOA in the presence of polymer sorbent are also evidence of the extent of molecular interaction. The ^{19}F resonances due to PFOA in Figure 4 broaden upon the addition of polymer (Table S1), mainly due to the restriction of mobility of the fluorinated segments on interacting with the polymer through fluorine−fluorine hydrophobic interactions and/or electrostatic attraction.[17,22,39] With increasing PFOA concentration >0.3 mM (still below the CMC), the ^{19}F NMR resonances of PFOA in the presence of the polymer shift back and approach the chemical shifts of free PFOA, indicating the effects of fast chemical exchange (Figures S7−S9).

^{19}F DOSY NMR provides additional understanding of the nature of fluorine−fluorine and electrostatic interactions by providing measurements of the self-diffusion coefficients (D_f) of PFOA and the polymer sorbent upon mixing.[22] In this work,

https://doi.org/10.1021/acs.macromol.1c02435
Macromolecules 2022, 55, 1077−1087

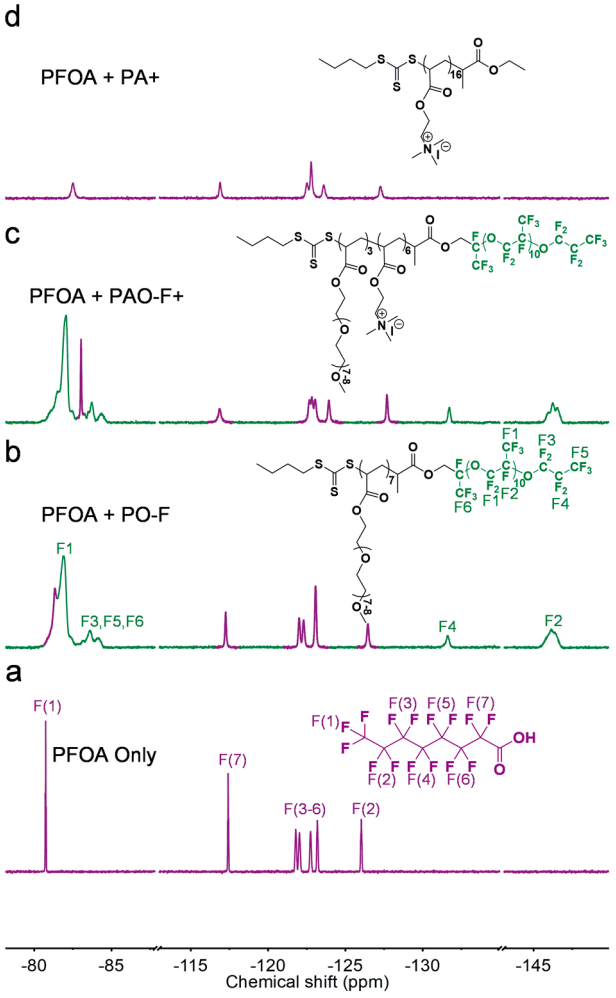

Figure 4. ^{19}F NMR spectra of 0.3 mM PFOA in the absence (a) and presence of polymer sorbent (b) PO-F (0.171 mM), (c) PAO-F+ (0.177 mM), and (d) PA+ (0.066 mM) in Milli-Q water. The mole ratio of PFOA to polymer is 1.8 for PO-F, 1.7 for PAO-F+, and 4.6 for PA+. The mole ratios of PFOA to the two PFPE-containing polymers are the same within experimental error.

D_f of free PFOA in Milli-Q water was measured to be 4.5 × 10^{-10} m^2/s (Table 2), corresponding to a hydrodynamic diameter of 1.1 nm calculated via the Stokes−Einstein equation (Table S2).[40] This indicates that PFOA molecules were fully solvated in solution. The self-diffusion coefficients of the two PFPE-containing polymers in the aqueous solutions were measured to be 3.6 × 10^{-11} and 6.4 × 10^{-11} m^2/s (Table 2) for PO-F and PAO-F+ and give hydrodynamic diameters of 14.3 and 8.1 nm, respectively (Table S2). The calculated hydrodynamic diameters of the two polymers agree with the results of the MD simulations discussed above, indicating that the polymer PAO-F+ with quaternary ammonium groups forms smaller aggregates than the nonionic polymer PO-F in the aqueous solution due to the effect of electrostatic repulsion between chains.

Table 2. Diffusion Coefficients (D_f) of PO-F and PAO-F+ Block Copolymers with and without the Presence of PFOA in Milli-Q Water; the Final Row Shows the Proportions of Unbound PFOA after Sorption by the Block Copolymers

	PO-F	PAO-F+			
mole ratio of PFOA to polymer	1.8	1.7	4.0	5.2	6.9
	D_f (× 10^{11} m^2/s)				
polymer only	3.6		6.4		
polymer after sorption	5.4	6.2	4.0	4.4	4.4
PFOA only			45.0		
PFOA after sorption	39	6.2	4.9	13.0	27.8
proportion of free PFOA (%)	84.8	0.0	2.2	21.2	57.6

The diffusion coefficients, D_f, after mixing PFOA with polymer sorbents are summarized in Table 2. At a mole ratio of PFOA to polymer PO-F of 1.8, the value of D_f of PFOA decreases slightly from 4.5 × 10^{-10} to 3.9 × 10^{-10} m^2/s (Figure 5a and Table S2). Such behavior indicates that PFOA is undergoing fast exchange between the solution and PO-F during the DOSY NMR time scale (diffusion time = 0.3 s) and is consistent with the findings reported in our previous work.[22] At the same time, an increase in D_f for PO-F was observed after sorption of PFOA, indicating a decreased hydrodynamic diameter from 14.3 to 9.5 nm (Table S2). This observation is in agreement with the MD simulations which supported partial demicellization of PO-F, resulting from enhanced electrostatic repulsion driven by the sorbed PFOA. A single self-diffusion coefficient was measured in all cases, indicating that PFOA is in fast exchange been "bound" and "free" states. The observed self-diffusion coefficient in the fast exchange regime is equal to the sum of D_f for the bound and free species, weighted by their number fractions. Therefore, the proportion of free PFOA was calculated to be 84.8% in this manner (Table 2) via eq 1.[41]

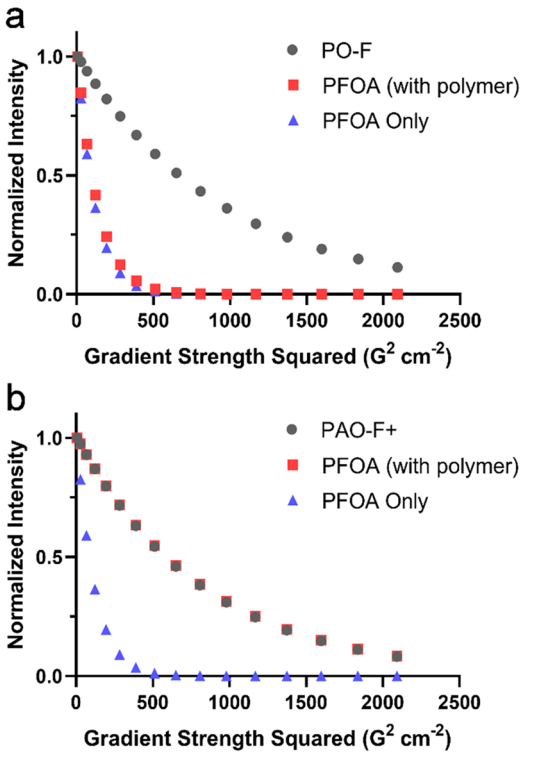

Figure 5. ^{19}F NMR DOSY decay curves of PFOA and sorbents (a) PO-F and (b) PAO-F+ in water at 25 °C. The mole ratio of PFOA to the two polymer sorbents was 1.8 for PO-F and 1.7 for PAO-F+.

$$D_{observed} = f_{free} D_{free} + (1 - f_{free}) D_{polymer} \quad (1)$$

https://doi.org/10.1021/acs.macromol.1c02435
Macromolecules 2022, 55, 1077−1087

where $D_{observed}$ is the D_f of PFOA in the presence of polymer, D_{free} is the D_f of PFOA without polymer, and $D_{polymer}$ is the D_f of the polymer in the presence of PFOA.

The diffusion coefficients, D_f, of cationic PAO-F+ and PFOA upon mixing at a mole ratio of PFOA to polymer of 1.7 underwent larger changes compared to those observed for PO-F on addition of PFOA. The self-diffusion coefficient of PFOA decreased by an order of magnitude, from 4.5×10^{-10} to 6.2×10^{-11} m^2/s, indicating that PFOA was diffusing at the same rate as the polymer PAO-F+ ($D_f = 6.2 \times 10^{-11}$ m^2/s) after sorption (Figure 5b and Table 2). Chemical exchange was not observed under such conditions, suggesting tight binding of PFOA to PAO-F+ due presumably to electrostatic attraction and indicating ~100% PFOA sorption. The DOSY results therefore suggest that the incorporation of cationic groups can significantly increase the strength of binding of PFOA to polymer sorbents, in agreement with previous findings.[20]

Fast exchange between bound and free PFOA can be observed with increased addition of PFOA to the PAO-F+ solution. When the mole ratio of PFOA to copolymer was increased from 1.7 to 4.0, the self-diffusion coefficient of PFOA was measured to be 4.9×10^{-11} m^2/s, an order of magnitude lower than D_f of free PFOA (4.5×10^{-10} m^2/s) and close to that of PAO-F+ (4.0×10^{-11} m^2/s) (Table 2 and Figure S10a). The proportion of free, unbound PFOA was calculated to be 2.2% by using eq 1, suggesting the reduced capture of PFOA via electrostatic attraction when the concentration of PFOA increases. The D_f of PFOA further increased to 1.30×10^{-10} and 2.78×10^{-10} m^2/s when the mole ratio was increased to 5.2 and 6.9, respectively, approaching the diffusion coefficient of free PFOA. The proportion of free PFOA was calculated to be 21.2 and 57.6%, respectively (Table 2 and Figure S10b,c). The increased proportion of free PFOA can be explained by an excess of PFOA that exceeds the sorption capacity of PAO-F+. The self-diffusion coefficient of PAO-F+ decreased from 6.2×10^{-11} to 4.0×10^{-11} m^2/s when the ratio of PFOA to polymer was 4.0 and then remained largely constant with further addition of PFOA. Unexpectedly, fast exchange occurs before the PAO-F+ reaches its theoretical neutralization point, that is, when the mole ratio of PFOA to PAO-F+ is 6.0. This indicates that, in addition to the sorption being driven by electrostatic attraction, fluorine−fluorine interactions also contribute to PFOA sorption, potentially increasing the PFOA removal capacity when both interactions are in effect.

Upon mixing PFOA with PA+, broad ^{19}F NMR peaks belonging to PFOA were observed due to decreased hydrophilicity/charge and formation of large aggregates,[34,42,43] agreeing well with the MD simulation results presented in Figure 3c. At the highest mole ratio of PFOA to PA+ of 29.1, two sets of peaks can be seen: a broad peak at −83.3 ppm assigned to the PFOA sorbed by PA+ and a second due to free PFOA (Figure S9). This observation suggests that the concentration of PFOA exceeds the binding capacity of PA+ and that the two populations of PFOA are not exchanging.

The ζ potential and hydrodynamic diameter (D_h) of the polymer sorbents change significantly with continuous addition of PFOA to the polymer solutions. To guide the discussion, Figure 6 has been labeled with five mole ratios of PFOA to polymer, namely, "A", "B", "C", "D", and "E" (see also Table 3 and Table S3). These ratios correspond to solutions used in the ^{19}F NMR measurements discussed above. Upon the addition of PFOA to the solution of PO-F, the ζ potential decreases immediately from neutral to negative (e.g., −4.1 and −9.1 mV at lines A and B, respectively), this being attributed to the presence of the sorbed anionic PFOA (Figure 6a). Meanwhile, a rapid decrease in polymer size from 8.6 to <5 nm was observed, suggesting disassembly of the PO-F micelles in the presence of PFOA, a result in good agreement with the changes in D_h calculated from the ^{19}F NMR DOSY experiments (Table S2) and with the results of the MD simulations.

The ζ potential of PAO-F+ without PFOA was measured to be ~30 mV. With continuous addition of PFOA, a steady

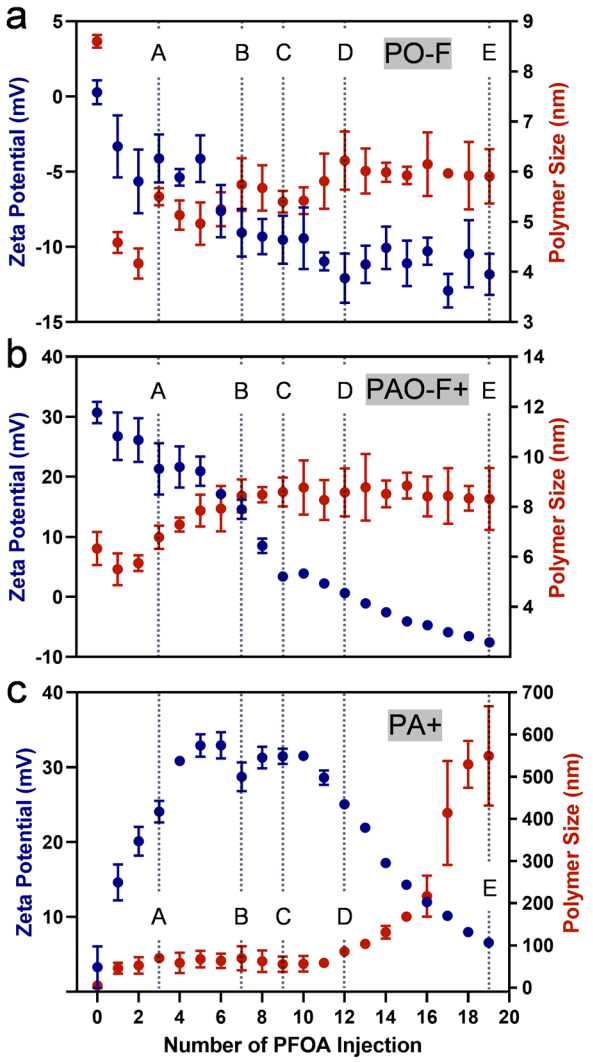

Figure 6. ζ potential and hydrodynamic size of the three polymer sorbents (a) PO-F, (b) PAO-F+, and (c) PA+ with continuous addition of PFOA at 25 °C. Blue: ζ potential values; red: size of polymer sorbent. Each size and ζ potential value are the average value of five measurements, and standard deviation is shown. "A", "B", "C" "D", and "E" indicate the five molar ratios of PFOA to polymer also used in the ^{19}F NMR analyses and listed in Table 3.

Table 3. Mole Ratios of PFOA to Polymer, Labeled as A−E in Figures 6 and 7

no. of PFOA injection	3 (A)	7 (B)	9 (C)	12 (D)	19 (E)
PFOA:PO-F	1.8	4.1	5.3	7.1	11.2
PFOA:PAO-F+	1.7	4.0	5.2	6.9	10.8
PFOA:PA+	4.6	10.7	13.8	18.3	29.1

https://doi.org/10.1021/acs.macromol.1c02435
Macromolecules 2022, 55, 1077−1087

decrease in ζ potential was observed due to the neutralization of the cationic groups of PAO-F+ by the anionic PFOA. The neutralization point was observed slightly above the mole ratio of PFOA to polymer of 6.9 (point "D" in Figure 6b), higher than the theoretical value of 6.0, likely due to the direct sorption of PFOA by the PFPE segments of PAO-F+. The hydrodynamic size of PAO-F+ continuously increased with increasing PFOA concentration, reaching 8.4 nm at a mole ratio of 4.0 ("B"). The polymer size was then maintained at ∼8.5 nm on further additions (positions "C", "D", and "E" in Figure 6b). Again, the results are broadly consistent with the hydrodynamic diameters calculated from the ^{19}F NMR DOSY experiments (Table S2).

Obvious changes in ζ and size of PA+ were also observed after mixing with PFOA in the aqueous solution. The non-PFPE polymer PA+ adopts a single-chain folding conformation and thus lacks a slipping plane that is essential for establishment of a ζ potential,[44,45] and so the measured initial value of ζ of the polymer without addition of PFOA is not reliable, showing a value of only 3.3 mV (Figure 6c). The lack of validity of the observed ζ value is also supported by the theoretical framework developed by Ohshima.[46] In his work, he demonstrated that for a rigid colloidal particle the electrophoretic mobility can be used for direct calculation of the ζ potential. However, for a soft polyelectrolyte lacking a rigid core, i.e., PA+, there is no clear relationship between electrophoretic mobility and ζ. Upon the first three additions of PFOA, an increase in ζ was observed, mainly caused by the formation of large aggregates gradually building a rigid core composed of perfluoroalkyl segments of PFOA, hence producing reliable ζ values of the polymer−PFOA aggregates. As was proposed again by Ohshima,[47] particles containing a rigid core covered with a soft polyelectrolyte layer show increased electrophoretic mobility and thus increased ζ with decreased thickness ratio of outer layer to the inner core. The influence of the size of the rigid core on the electrophoretic mobility of the particle is not significant outside of a thickness ratio of 10^{-2} to 1. Consequently, the increase in ζ can be attributed to a significantly increased size of the hydrophobic core with further additions of PFOA to the polymer solution. Beyond the point "A", the ζ potential remained constant at ∼30 mV to point "C" and then decreased with increasing PFOA concentration. The theoretical neutralization point for this system should be at a mole ratio of 16.0; however, neutralization was not achieved even after the addition of a large excess of PFOA of >29. This could be explained by the direct sorption of PFOA by the polymer−PFOA aggregates via fluorine−fluorine interactions that do not contribute to the value of the ζ potential. Direct capture of PFOA molecules by perfluoroalkyl segments has been previously reported.[17,39,48] Notably, large multiple chain aggregates (>80 nm) are formed upon the continuous addition of PFOA up to the mole ratio "D" (Figure 6c), again corresponding well with the findings in the MD simulations and ^{19}F NMR DOSY experiments. A significant increase in particle size to >550 nm was seen with further addition of PFOA, in line with the decrease in ζ, leading to decreased solubility and stability of the aggregated PA+.[49]

Isothermal titration calorimetry (ITC) offers real-time analysis of thermodynamic interactions between PFOA and the polymer sorbent by titrating PFOA into the corresponding polymer solutions.[50−53] The amount of PFOA injected at each point was controlled so that the mole ratio of PFOA to polymer was the same as in the DLS experiments discussed above. The ITC raw traces in Figures S11−S13 (black curve) are composed of 19 spikes due to 19 additions, with the full width of each spike indicating the time scale of the interaction between PFOA and the polymer.[54] The sorption duration was fully completed within the preset injection interval, i.e., 250 s upon each PFOA injection, suggesting a rapid (<5 min) sorption of PFOA by the three polymers. Thermograms due to the interactions between PFOA and each polymer sorbent, after subtraction of the blank experiment, i.e., PFOA titrated into Milli-Q water, are shown in Figure 7. A negative ΔH is

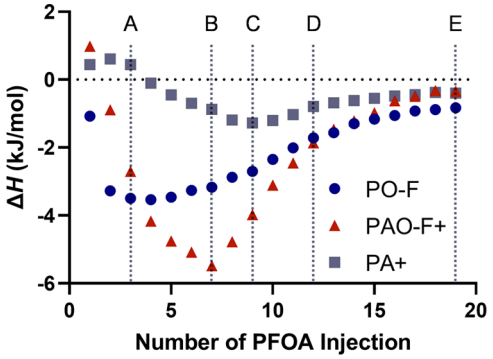

Figure 7. ITC thermograms of interaction of PFOA with the three polymers in Milli-Q water at 25 °C. The points "A", "B", "C", "D", and "E" are the same five mole ratios of PFOA to the three polymers as in Figure 6.

observed in the thermogram of PO-F throughout the total 19 PFOA injections (Figure 7, in blue), demonstrating exothermic events due to the fluorine−fluorine interactions. Similar observations of negative ΔH on hydrophobic interactions were reported by others.[55,56] For polymers bearing cationic quaternary ammonium groups, endothermic events are observed for titration of PFOA into solutions of both PAO-F + (first injection) and PA+ (first three injections) (Figures 7, in red and gray), indicating the presence of an endothermic event arising from the electrostatic attraction between PFOA and the two cationic polymers. This is in line with the report by Skvarnavičius et al.,[57] who observed endothermic binding interactions by titrating cationic alkylamines surfactant solution into a solution containing anionic poly(amino acid)s with carboxyl groups.

The enthalpies ΔH in the ITC thermograms are the summation of the contributions from two interaction processes, namely (1) interactions between PFOA and polymer and (2) changes in aggregation size. The decrease in ΔH on the first several additions of the solutions of PFOA to PO-F (Figure 7, in blue) can be attributed to the disaggregation of the polymeric micelles, as also indicated by the MD simulations and DLS measurements. After incorporation of cationic groups in PAO-F+, the thermogram in Figure 7 shows that before point "A", a switch from an initial endothermic event upon the first PFOA injection to an exothermic event after the second injection can be observed, indicating that with presence of both fluorine−fluorine and electrostatic attractions the electrostatic attractions dominated upon the first injection. The finding corresponds well with the work of Khan and Brettmann,[58] who concluded a priority of electrostatic attraction over hydrophobic interactions between anionic surfactant and cationic polymer when the polymer is

https://doi.org/10.1021/acs.macromol.1c02435
Macromolecules 2022, 55, 1077−1087

highly charged. A continuous decrease in ΔH until a mole ratio of PFOA to the polymer of 4.0 was observed, mainly due to the attenuated electrostatic attraction between PFOA and the polymer with increasing addition of PFOA, as confirmed by the ζ potential measurements (Figure 6b), and further supports our findings from the DOSY experiments. Compared with PAO-F+ which only shows the first injection to be endothermic (Figure 7, in red), the titration of PFOA into PA+ displays endothermic events for the first three PFOA injections (Figure 7, in gray). This highlights the role of fluorine−fluorine interactions in the fluorinated block copolymer PAO-F+. In summary, the results from the ITC agree well with the DLS results and provide a clear description of the changes in aggregation of the polymers in the presence of increasing amounts of PFOA.

CONCLUSIONS

This study has demonstrated that fluorine−fluorine interactions and electrostatic attraction play important roles in determining the mechanism of interaction of PFOA with three novel block copolymer sorbents. Three classes of polymers were successfully prepared, namely neutral PFPE-containing polymer PO-F, cationic PFPE-containing polymer PAO-F+, and cationic non-PFPE polymer PA+. Upon mixing PFOA with aqueous solutions of the polymer sorbents, both PFPE and quaternary ammonium groups contribute significantly to the effective and rapid (<5 min) sorption of PFOA as confirmed through molecular dynamics simulations, ^{19}F NMR, DLS, and isothermal titration calorimetry. We observed that PFOA involved in fluorine−fluorine interactions undergoes fast exchange between the bound and free states while the electrostatic interactions result in tight binding of PFOA without measurable chemical exchange. When both PFPE and cationic groups are present, the fluorine−fluorine interactions can augment the effect of electrostatic attraction for direct sorption of PFOA in the solution, potentially improving PFOA sorption capacity of the polymer sorbent. Additionally, the electrostatic attraction between PFOA and the cationic fluorinated sorbent is strong and dominant for sorption of PFOA at low concentrations. Overall, this work presents important rules for the design of sorbents for rapid and efficient PFAS removal from contaminated aqueous solutions. Future work will focus on applying these design rules to prepare PFPE-based magnetic iron oxide nanoparticles and membranes for remediation of PFAS at environmentally relevant conditions.

ASSOCIATED CONTENT

Supporting Information

The Supporting Information is available free of charge at https://pubs.acs.org/doi/10.1021/acs.macromol.1c02435.

Synthetic procedures, ^{1}H NMR and ^{19}F NMR spectra with assignments, PFOA peak widths at half-height (in ppm) from ^{19}F NMR spectra, D_h of PO-F and PAO-F+ with and without the presence of different concentrations of PFOA calculated from ^{19}F NMR DOSY, ^{19}F NMR DOSY decay curves of PAO-F+ with the presence of different concentrations of PFOA, listed series of concentrations of PFOA and the three polymers, ITC raw traces of the three polymers titrated by PFOA (PDF)

AUTHOR INFORMATION

Corresponding Authors

Cheng Zhang − *Australian Institute for Bioengineering and Nanotechnology, The University of Queensland, Brisbane, QLD 4072, Australia; ARC Centre of Excellence in Convergent Bio-Nano Science and Technology, The University of Queensland, Brisbane, QLD 4072, Australia;* orcid.org/0000-0002-2722-7497; Email: c.zhang3@uq.edu.au

Andrew K. Whittaker − *Australian Institute for Bioengineering and Nanotechnology, The University of Queensland, Brisbane, QLD 4072, Australia; ARC Centre of Excellence in Convergent Bio-Nano Science and Technology, The University of Queensland, Brisbane, QLD 4072, Australia;* orcid.org/0000-0002-1948-8355; Email: a.whittaker@uq.edu.au

Authors

Xiao Tan − *Australian Institute for Bioengineering and Nanotechnology, The University of Queensland, Brisbane, QLD 4072, Australia; ARC Centre of Excellence in Convergent Bio-Nano Science and Technology, The University of Queensland, Brisbane, QLD 4072, Australia*

Michał Sawczyk − *Department of Chemistry, University of Illinois at Chicago, Chicago, Illinois 60607, United States*

Yixin Chang − *Australian Institute for Bioengineering and Nanotechnology, The University of Queensland, Brisbane, QLD 4072, Australia; ARC Centre of Excellence in Convergent Bio-Nano Science and Technology, The University of Queensland, Brisbane, QLD 4072, Australia*

Yiqing Wang − *Australian Institute for Bioengineering and Nanotechnology, The University of Queensland, Brisbane, QLD 4072, Australia*

Adil Usman − *Australian Institute for Bioengineering and Nanotechnology, The University of Queensland, Brisbane, QLD 4072, Australia; ARC Centre of Excellence in Convergent Bio-Nano Science and Technology, The University of Queensland, Brisbane, QLD 4072, Australia*

Changkui Fu − *Australian Institute for Bioengineering and Nanotechnology, The University of Queensland, Brisbane, QLD 4072, Australia; ARC Centre of Excellence in Convergent Bio-Nano Science and Technology, The University of Queensland, Brisbane, QLD 4072, Australia;* orcid.org/0000-0002-2444-607X

Petr Král − *Department of Chemistry, University of Illinois at Chicago, Chicago, Illinois 60607, United States; Department of Physics, University of Illinois at Chicago, Chicago, Illinois 60607, United States; Department of Pharmaceutical Sciences, University of Illinois at Chicago, Chicago, Illinois 60612, United States;* Present Address: Department of Chemical Engineering, University of Illinois at Chicago, Chicago, Illinois 60608, United States; orcid.org/0000-0003-2992-9027

Hui Peng − *Australian Institute for Bioengineering and Nanotechnology, The University of Queensland, Brisbane, QLD 4072, Australia; ARC Centre of Excellence in Convergent Bio-Nano Science and Technology, The University of Queensland, Brisbane, QLD 4072, Australia*

Complete contact information is available at: https://pubs.acs.org/10.1021/acs.macromol.1c02435

Notes

The authors declare no competing financial interest.

https://doi.org/10.1021/acs.macromol.1c02435
Macromolecules 2022, 55, 1077−1087

■ ACKNOWLEDGMENTS

The authors acknowledge the Australian Research Council (CE140100036, DP0987407, DP110104299, DP130103774, DP180101221, DP210101496, LE0775684, LE0668517, and LE0882357) and the National Health and Medical Research Council (APP1021759, APP1046831, APP1107723, and APP1158026) for funding of this research. C.Z. acknowledges the National Health and Medical Research Council for his Early Career Fellowship (APP1157440). C.F. acknowledges the University of Queensland for a UQ Development Fellowship (UQFEL1831361). The Australian National Fabrication Facility, Queensland Node, is acknowledged for access to some items of equipment. The Chemours Company is also acknowledged for providing perfluorinated poly(propylene ether).

■ REFERENCES

(1) Cousins, I. T.; DeWitt, J. C.; Gluge, J.; Goldenman, G.; Herzke, D.; Lohmann, R.; Ng, C. A.; Scheringer, M.; Wang, Z. Y. The high persistence of PFAS is sufficient for their management as a chemical class. *Environ. Sci.: Process. Impacts* **2020**, *22*, 2307−2312.

(2) Schaider, L. A.; Balan, S. A.; Blum, A.; Andrews, D. Q.; Strynar, M. J.; Dickinson, M. E.; Lunderberg, D. M.; Lang, J. R.; Peaslee, G. F. Fluorinated Compounds in U.S. Fast Food Packaging. *Environ. Sci. Technol. Lett.* **2017**, *4*, 105−111.

(3) Steindal, E. H.; Grung, M. Management of PFAS with the aid of chemical product registries-an indispensable tool for future control of hazardous substances. *Integr. Environ. Assess. Manag.* **2021**, *17*, 835−851.

(4) Kotthoff, M.; Muller, J.; Jurling, H.; Schlummer, M.; Fiedler, D. Perfluoroalkyl and polyfluoroalkyl substances in consumer products. *Environ. Sci. Pollut. Res.* **2015**, *22*, 14546−14559.

(5) Herzke, D.; Olsson, E.; Posner, S. Perfluoroalkyl and polyfluoroalkyl substances (PFASs) in consumer products in Norway - A pilot study. *Chemosphere* **2012**, *88*, 980−987.

(6) Hoover, G.; Kar, S.; Guffey, S.; Leszczynski, J.; Sepulveda, M. S. In vitro and in silico modeling of perfluoroalkyl substances mixture toxicity in an amphibian fibroblast cell line. *Chemosphere* **2019**, *233*, 25−33.

(7) de Vries, P.; Slijkerman, D. M. E.; Kwadijk, C.; Kotterman, M. J. J.; Posthuma, L.; de Zwart, D.; Murk, A. J.; Foekema, E. M. The toxic exposure of flamingos to per- and Polyfluoroalkyl substances (PFAS) from firefighting foam applications in Bonaire. *Mar. Pollut. Bull.* **2017**, *124*, 102−111.

(8) Haukas, M.; Berger, U.; Hop, H.; Gulliksen, B.; Gabrielsen, G. W. Bioaccumulation of per- and polyfluorinated alkyl substances (PFAS) in selected species from the Barents Sea food web. *Environ. Pollut.* **2007**, *148*, 360−371.

(9) Zhang, C.; Yan, K.; Fu, C.; Peng, H.; Hawker, C. J.; Whittaker, A. K. Biological Utility of Fluorinated Compounds: from Materials Design to Molecular Imaging, Therapeutics and Environmental Remediation. *Chem. Rev.* **2022**, *122*, 167−208.

(10) Newell, C. J.; Adamson, D. T.; Kulkarni, P. R.; Nzeribe, B. N.; Stroo, H. Comparing PFAS to other groundwater contaminants: Implications for remediation. *Remediation* **2020**, *30*, 7−26.

(11) Mahinroosta, R.; Senevirathna, L. A review of the emerging treatment technologies for PFAS contaminated soils. *J. Environ. Manage.* **2020**, *255*, 109896.

(12) McCleaf, P.; Englund, S.; Ostlund, A.; Lindegren, K.; Wiberg, K.; Ahrens, L. Removal efficiency of multiple poly- and perfluoroalkyl substances (PFASs) in drinking water using granular activated carbon (GAC) and anion exchange (AE) column tests. *Water Res.* **2017**, *120*, 77−87.

(13) Boyer, T. H.; Fang, Y.; Ellis, A.; Dietz, R.; Choi, Y. J.; Schaefer, C. E.; Higgins, C. P.; Strathmann, T. J. Anion exchange resin removal of per- and polyfluoroalkyl substances (PFAS) from impacted water: A critical review. *Water Res.* **2021**, *200*, 117244.

(14) Cummings, L.; Matarazzo, A.; Nelson, N.; Sickels, F.; Storms, C. Recommendation on perfluorinated compound treatment options for drinking water; New Jersey Drinking Water Quality Institute Treatment Subcommittee Report, New Jersey, 2015.

(15) Appleman, T. D.; Higgins, C. P.; Quinones, O.; Vanderford, B. J.; Kolstad, C.; Zeigler-Holady, J. C.; Dickenson, E. R. Treatment of poly- and perfluoroalkyl substances in U.S. full-scale water treatment systems. *Water Res.* **2014**, *51*, 246−255.

(16) Eriksson, P. Nanofiltration extends the range of membrane filtration. *Environ. Prog.* **1988**, *7*, 58−62.

(17) Koda, Y.; Terashima, T.; Sawamoto, M. Fluorous microgel star polymers: selective recognition and separation of polyfluorinated surfactants and compounds in water. *J. Am. Chem. Soc.* **2014**, *136*, 15742−15748.

(18) Shetty, D.; Jahovic, I.; Skorjanc, T.; Erkal, T. S.; Ali, L.; Raya, J.; Asfari, Z.; Olson, M. A.; Kirmizialtin, S.; Yazaydin, A. O.; Trabolsi, A. Rapid and Efficient Removal of Perfluorooctanoic Acid from Water with Fluorine-Rich Calixarene-Based Porous Polymers. *ACS Appl. Mater. Interfaces* **2020**, *12*, 43160−43166.

(19) Yang, A.; Ching, C.; Easler, M.; Helbling, D. E.; Dichtel, W. R. Cyclodextrin Polymers with Nitrogen-Containing Tripodal Cross-linkers for Efficient PFAS Adsorption. *ACS Mater. Lett.* **2020**, *2*, 1240−1245.

(20) Kumarasamy, E.; Manning, I. M.; Collins, L. B.; Coronell, O.; Leibfarth, F. A. Ionic Fluorogels for Remediation of Per- and Polyfluorinated Alkyl Substances from Water. *ACS Cent. Sci.* **2020**, *6*, 487−492.

(21) Whittaker, A.; Zhang, C.; Tan, X. Capture of Fluorinated Carbon Compounds. WO 2020160626 A1, February 7, 2020.

(22) Tan, X.; Zhong, J.; Fu, C.; Dang, H.; Han, Y.; Král, P.; Guo, J.; Yuan, Z.; Peng, H.; Zhang, C.; Whittaker, A. K. Amphiphilic Perfluoropolyether Copolymers for the Effective Removal of Polyfluoroalkyl Substances from Aqueous Environments. *Macromolecules* **2021**, *54*, 3447−3457.

(23) Ferguson, C. J.; Hughes, R. J.; Nguyen, D.; Pham, B. T.; Gilbert, R. G.; Serelis, A. K.; Such, C. H.; Hawkett, B. S. Ab initio emulsion polymerization by RAFT-controlled self-assembly. *Macromolecules* **2005**, *38*, 2191−2204.

(24) Zhang, C.; Moonshi, S. S.; Han, Y.; Puttick, S.; Peng, H.; Magoling, B. J. A.; Reid, J. C.; Bernardi, S.; Searles, D. J.; Kral, P.; Whittaker, A. K. PFPE-Based Polymeric ^{19}F MRI Agents: A New Class of Contrast Agents with Outstanding Sensitivity. *Macromolecules* **2017**, *50*, 5953−5963.

(25) Zhang, C.; Li, L.; Han, F. Y.; Yu, X.; Tan, X.; Fu, C.; Xu, Z. P.; Whittaker, A. K. Integrating Fluorinated Polymer and Manganese-Layered Double Hydroxide Nanoparticles as pH-activated ^{19}F MRI Agents for Specific and Sensitive Detection of Breast Cancer. *Small* **2019**, *15*, No. e1902309.

(26) Phillips, J. C.; Braun, R.; Wang, W.; Gumbart, J.; Tajkhorshid, E.; Villa, E.; Chipot, C.; Skeel, R. D.; Kale, L.; Schulten, K. Scalable molecular dynamics with NAMD. *J. Comput. Chem.* **2005**, *26*, 1781−1802.

(27) Vanommeslaeghe, K.; Raman, E. P.; MacKerell, A. D., Jr. Automation of the CHARMM General Force Field (CGenFF) II: Assignment of bonded parameters and partial atomic charges. *J. Chem. Inf. Model.* **2012**, *52*, 3155−3168.

(28) Yu, W.; He, X.; Vanommeslaeghe, K.; MacKerell, A. D., Jr. Extension of the CHARMM General Force Field to Sulfonyl-Containing Compounds and Its Utility in Biomolecular Simulations. *J. Comput. Chem.* **2012**, *33*, 2451−2468.

(29) Darden, T.; York, D.; Pedersen, L. Particle Mesh Ewald - an N. Log(N) Method for Ewald Sums in Large Systems. *J. Chem. Phys.* **1993**, *98*, 10089−10092.

(30) Johansson, J. H.; Yan, H.; Berger, U.; Cousins, I. T. Water-to-air transfer of branched and linear PFOA: Influence of pH, concentration and water type. *Emerg. Contam.* **2017**, *3*, 46−53.

(31) Goss, K. U. The pKa Values of PFOA and Other Highly Fluorinated Carboxylic Acids. *Environ. Sci. Technol.* **2008**, *42*, 456−458.

https://doi.org/10.1021/acs.macromol.1c02435
Macromolecules 2022, 55, 1077−1087

(32) Truong, N. P.; Jia, Z.; Burges, M.; McMillan, N. A.; Monteiro, M. J. Self-catalyzed degradation of linear cationic poly(2-dimethylaminoethyl acrylate) in water. *Biomacromolecules* **2011**, *12*, 1876−1882.
(33) Chen, A.; Er, G.; Zhang, C.; Tang, J.; Alam, M.; Ta, H. T.; Elliott, A. G.; Cooper, M. A.; Perera, J.; Swift, S.; Blakey, I.; Whittaker, A. K.; Peng, H. Antimicrobial anilinium polymers: The properties of poly (N, N-dimethylaminophenylene methacrylamide) in solution and as coatings. *J. Polym. Sci., Part A: Polym. Chem.* **2019**, *57*, 1908−1921.
(34) Zhang, C.; Peng, H.; Whittaker, A. K. NMR investigation of effect of dissolved salts on the thermoresponsive behavior of oligo (ethylene glycol)-methacrylate-based polymers. *J. Polym. Sci., Part A: Polym. Chem.* **2014**, *52*, 2375−2385.
(35) Zhang, C.; Peng, H.; Puttick, S.; Reid, J.; Bernardi, S.; Searles, D. J.; Whittaker, A. K. Conformation of Hydrophobically Modified Thermoresponsive Poly(OEGMA-Co-TFEA) across the LCST Revealed by NMR and Molecular Dynamics Studies. *Macromolecules* **2015**, *48*, 3310−3317.
(36) Usman, A.; Zhang, C.; Zhao, J.; Peng, H.; Kurniawan, N. D.; Fu, C.; Hill, D. J.; Whittaker, A. K. Tuning the thermoresponsive properties of PEG-based fluorinated polymers and stimuli responsive drug release for switchable ^{19}F magnetic resonance imaging. *Polym. Chem.* **2021**, *12*, 5438−5448.
(37) Zhang, C.; Moonshi, S. S.; Peng, H.; Puttick, S.; Reid, J.; Bernardi, S.; Searles, D. J.; Whittaker, A. K. Ion-Responsive ^{19}F MRI Contrast Agents for the Detection of Cancer Cells. *ACS Sens.* **2016**, *1*, 757−765.
(38) Harada, K.; Xu, F.; Ono, K.; Iijima, T.; Koizumi, A. Effects of PFOS and PFOA on L-type Ca^{2+} currents in guinea-pig ventricular myocytes. *Biochem. Biophys. Res. Commun.* **2005**, *329*, 487−494.
(39) Koda, Y.; Terashima, T.; Nomura, A.; Ouchi, M.; Sawamoto, M. Fluorinated microgel-core star polymers as fluorous compartments for molecular recognition. *Macromolecules* **2011**, *44*, 4574−4578.
(40) Zhang, C.; Sanchez, R. J. P.; Fu, C.; Clayden-Zabik, R.; Peng, H.; Kempe, K.; Whittaker, A. K. Importance of Thermally Induced Aggregation on ^{19}F Magnetic Resonance Imaging of Perfluoropolyether-Based Comb-Shaped Poly(2-oxazoline)s. *Biomacromolecules* **2019**, *20*, 365−374.
(41) Truong, N. P.; Zhang, C.; Nguyen, T. A.; Anastasaki, A.; Schulze, M. W.; Quinn, J. F.; Whittaker, A. K.; Hawker, C. J.; Whittaker, M. R.; Davis, T. P. Overcoming surfactant-induced morphology instability of noncrosslinked diblock copolymer nano-objects obtained by RAFT emulsion polymerization. *ACS Macro Lett.* **2018**, *7*, 159−165.
(42) Joshi, S.; Khatri, L. R.; Kumar, A.; Rathore, A. S. Monitoring size and oligomeric-state distribution of therapeutic mAbs by NMR and DLS: Trastuzumab as a case study. *J. Pharm. Biomed. Anal.* **2021**, *195*, 113841.
(43) Aksnes, D.; Gjerdåker, L. NMR line width, relaxation and diffusion studies of cyclohexane confined in porous silica. *J. Mol. Struct.* **1999**, *475*, 27−34.
(44) Bhattacharjee, S. DLS and zeta potential-what they are and what they are not? *J. Controlled Release* **2016**, *235*, 337−351.
(45) Salopek, B.; Krasic, D.; Filipovic, S. Measurement and application of zeta-potential. *Rud. Zb.* **1992**, *4*, 147−151.
(46) Ohshima, H. Electrophoretic Mobility of Soft Particles. *Colloids Surf. A: Physicochem. Eng. Asp.* **1995**, *103*, 249−255.
(47) Ohshima, H. Electrophoretic Mobility of Soft Particles. *J. Colloid Interface Sci.* **1994**, *163*, 474−483.
(48) Quan, Q.; Wen, H.; Han, S.; Wang, Z.; Shao, Z.; Chen, M. Fluorous-Core Nanoparticle-Embedded Hydrogel Synthesized via Tandem Photo-Controlled Radical Polymerization: Facilitating the Separation of Perfluorinated Alkyl Substances from Water. *ACS Appl. Mater. Interfaces* **2020**, *12*, 24319−24327.
(49) Chauhan, S.; Kaur, M. Modulation of Aggregation Behaviour of Anionic Surfactant in the Presence of Aqueous Quaternary Ammonium Salts. *J. Surfactants Deterg.* **2017**, *20*, 599−607.
(50) Archer, W. R.; Schulz, M. D. Isothermal titration calorimetry: practical approaches and current applications in soft matter. *Soft Matter* **2020**, *16*, 8760−8774.
(51) Prozeller, D.; Morsbach, S.; Landfester, K. Isothermal titration calorimetry as a complementary method for investigating nanoparticle-protein interactions. *Nanoscale* **2019**, *11*, 19265−19273.
(52) Saponaro, A. Isothermal Titration Calorimetry: A Biophysical Method to Characterize the Interaction between Label-free Biomolecules in Solution. *Bio Protoc* **2018**, *8*, No. e2957.
(53) Xu, M.; Wan, J.; Niu, Q.; Liu, R. PFOA and PFOS interact with superoxide dismutase and induce cytotoxicity in mouse primary hepatocytes: A combined cellular and molecular methods. *Environ. Res.* **2019**, *175*, 63−70.
(54) Di Trani, J. M.; Moitessier, N.; Mittermaier, A. K. Measuring Rapid Time-Scale Reaction Kinetics Using Isothermal Titration Calorimetry. *Anal. Chem.* **2017**, *89*, 7022−7030.
(55) Wu, L.-L.; Gao, H.-W.; Gao, N.-Y.; Chen, F.-F.; Chen, L. Interaction of perfluorooctanoic acid with human serum albumin. *BMC Struct. Biol.* **2009**, *9*, 1−7.
(56) Maso, L.; Trande, M.; Liberi, S.; Moro, G.; Daems, E.; Linciano, S.; Sobott, F.; Covaceuszach, S.; Cassetta, A.; Fasolato, S.; Moretto, L. M.; De Wael, K.; Cendron, L.; Angelini, A. Unveiling the binding mode of perfluorooctanoic acid to human serum albumin. *Protein Sci.* **2021**, *30*, 830−841.
(57) Skvarnavičius, G.; Dvareckas, D.; Matulis, D.; Petrauskas, V. Thermodynamics of Interactions Between Charged Surfactants and Ionic Poly(amino acids) by Isothermal Titration Calorimetry. *Acs Omega* **2019**, *4*, 17527−17535.
(58) Khan, N.; Brettmann, B. Intermolecular Interactions in Polyelectrolyte and Surfactant Complexes in Solution. *Polymers* **2019**, *11*, 51.

https://doi.org/10.1021/acs.macromol.1c02435
Macromolecules 2022, 55, 1077−1087